Dopant profiling based on scanning electron and helium ion microscopy

A.K.W. Chee[a*] and S. A. Boden[b]

[a]Centre for Advanced Photonics and Electronics, Electrical Engineering Division, Department of Engineering, University of Cambridge, 9 JJ Thomson Avenue, Cambridge CB3 0FA, U.K.

[b]University of Southampton, Electronics and Computer Science, Highfield, Southampton SO17 1BJ, U.K.

Highlights

- Strong doping contrast from *n*-type regions in the SHIM without energy-filtering.
- Sensitivity limits are established of the SHIM and SEM techniques.
- We discuss the impact of SHIM imaging conditions on quantitative dopant profiling.
- Doping contrast stems from different surface layer thicknesses in the SHIM and SEM.

In this paper, we evaluate and compare doping contrast generated inside the scanning electron microscope (SEM) and scanning helium ion microscope (SHIM). Specialised energy-filtering techniques are often required to produce strong doping contrast to map donor distributions using the secondary electron (SE) signal in the SEM. However, strong doping contrast can be obtained from *n*-type regions in the SHIM, even without energy-filtering. This SHIM technique is more sensitive than the SEM to donor density changes above its sensitivity threshold, *i.e.* 10^{16} or 10^{17} donors cm^{-3} respectively on specimens with or without a *p-n* junction; its sensitivity limit is well above 2×10^{17} acceptors cm^{-3} on specimens with or without a *p-n* junction. Good correlation is found between the widths and slopes of experimentally measured doping contrast profiles of thin *p*-layers and the calculated widths and slopes of the potential energy distributions across these layers, at a depth of 1 – 3 nm and 5 – 10 nm below the surface in the SHIM and the SEM respectively. This is consistent with the mean escape depth of SEs in silicon being about 1.8 nm and 7 nm in the SHIM and SEM respectively, and we conclude that short escape depth, low energy SE signals are most suitable for donor profiling.

Keywords: Doping contrast; Secondary electron energy-filtering; Sensitivity limit; Electric potentials; Escape depth; p-n junction

*Corresponding author.
Email address: kwac2@cam.ac.uk (A.K.W. Chee)

I. INTRODUCTION

The future of the semiconductor industry depends critically on the ability to map dopants rapidly at high spatial resolution, and with high sensitivity. New spectroscopic techniques are in considerable demand to cope with the advent of next generation semiconductor devices having ultra-shallow junctions. Hence, dopant profiling at a resolution of sub-10 nm and detection sensitivity over a range of ~10^{16} – 10^{20} dopants cm^{-3} are important requisites.

Using a scanning electron microscope (SEM), it is possible to provide a rapid and contactless technique for the two-dimensional mapping of electrically active dopant profiles based on SE doping contrast (Perovic *et al.*, 1995; Turan *et al.*, 1996; Castell *et al.*, 1999; Sealy *et al*., 2000; Elliott *et al.*, 2002). Under standard imaging conditions, the *p*-type regions appear bright and the *n*-type regions appear dark, therefore doping contrast can be used to determine the position of electrical *p*-*n* junctions. The doping contrast mechanism is due to the built-in electric field across a *p*-*n* junction, modified by the effects of surface band-bending and external patch fields as the SEs are scattered by the surface electric potentials (Chee *et al.*, 2011). Oatley *et al.* (1957) first studied SE doping contrast from *p*-*n* junctions where it was shown that reverse biasing enhances contrast by changing the electric potentials of the semiconductor. Since then, recent developments in instrumentation have hitherto evolved the application of doping contrast to quantitative dopant profiling in the SEM at the required high spatial resolution, sensitivity and quantification accuracy. A resolution up to 1 nm is achievable (Elliott *et al.*, 2002), and sensitivity to dopant concentrations ranging from 10^{14} up to 10^{20} dopants cm^{-3} can be obtained at a quantification accuracy of at least ± 3 % (Perovic *et al.*, 1998; Venables *et al.*, 1998; Sealy *et al.*, 2000; Elliott *et al.*, 2002, Chee, 2009). As SE doping contrast is able to characterise dopants with high sensitivity over the required range and resolution, it is highly viable compared to a number of alternative techniques of limited range and resolution, are time-consuming, costly or destructive, or provide only 1-D measurements (*e.g.* spreading resistance profiling, secondary ion mass spectroscopy, atom probe tomography or scanning capacitance microscopy).

It is known that the SHIM can also be used to obtain SE doping contrast from semiconductors (Notte, 2008). Compared with an SEM, smaller spot sizes can be produced of the He^+ probe than of an electron probe owing to an atomically-sharp ion source and the heavier mass - thus shorter de Broglie wavelength - of the ions. Moreover, the He^+ ions do not scatter as widely in the specimen upon beam impingement, consequently yielding a narrower interaction radius and highly localised SE emission. Hence, superior spatial resolution can in principle be achieved using the SHIM at the sub-nanometre scale. However, previous work (*e.g.* Jepson *et al.*, 2011) showed that, despite the smaller probe size, using the SHIM rather than the SEM may not lead to an increase in the resolution of the doping contrast technique because according to Chee *et al.*, 2007 the resolution is limited to the electric potential distribution at the semiconductor surface modified by surface band-bending (see also Chee, 2009). For future devices having ultra-shallow junctions and high doping concentrations, we need to know how the number of dopants changes within a few nanometres, therefore a suitably fine probe size may be beneficial for resolution as changes in electric potentials are confined within nanometre length-scales across the junction space charges. As dopant mapping relies on a relative change in the SE intensity between different doped regions, using the SHIM is expected to be advantageous because the SE yield is more sensitive to

the material when induced by He^+ ions than by electron beam irradiation (Ward *et al.*, 2006; Inai *et al.* 2007).

Previous work on SE doping contrast using the SHIM has also focussed on mapping of acceptor dopant densities whereas no work has been demonstrated to date on mapping donors. Invariably, mapping of donor distributions may require specialised energy-filtering techniques to produce strong SE doping contrast in the SEM (Chee *et al.*, 2009; Schojahn *et al.*, 2002). Hence, it is instructive to investigate the potential of SHIM dopant profiling without the need for energy-filtering.

II. METHODS AND MATERIALS

The silicon structures studied comprise a series of *p*- or *n*-layers with widths ranging from approximately 100 nm to 1 μm and doping levels ranging from ~ 2×10^{16} to 3×10^{19} dopants cm^{-3}. These are summarised in Table 1.

No.	**Doped multilayers**	**Spacer and capping layers**	**Substrate**
1	Boron-doped *p*-type silicon, acceptor density varies from 2×10^{17} to 3×10^{19} cm^{-3}	Nominally undoped silicon	Antimony-doped *n*-type silicon, donor density is 5×10^{18} cm^{-3}
2	Boron-doped *p*-type silicon, acceptor density varies from 1.5×10^{17} to 8×10^{18} cm^{-3}	Boron-doped *p*-type silicon, acceptor density is 10^{17} cm^{-3}	Boron-doped *p*-type silicon, acceptor density is 5×10^{14} cm^{-3}
3	Phosphorus-doped *n*-type silicon, donor density varies from 3×10^{16} to 2×10^{19} cm^{-3}	Nominally undoped silicon	Boron-doped *p*-type silicon, acceptor density is 5×10^{14} cm^{-3}
4	Antimony-doped *n*-type silicon, donor density varies from 2×10^{16} to 8×10^{18} cm^{-3}	Nominally undoped silicon	Antimony-doped *n*-type silicon, donor density is 5×10^{18} cm^{-3}

Table 1: Four-types of multilayer specimens studied.

The epitaxial silicon layers were grown using a chemical vapour deposition (CVD) technique with dopants incorporated during growth. An operating temperature of ~ 1123 K was used to grow layers into silicon wafers along the [001] direction at a growth rate of ~ 0.15 μm/min under atmospheric pressure. There are two categories of *p*- or *n*-layer specimens: those grown on a *p*- or *n*-type silicon substrate. *N*-layer structures on an *n*-substrate have a thin silicon-germanium marker (~ 100 nm thick; 5 atomic % germanium) grown directly on the substrate before the intentionally-doped epi-layers. The capping and spacer layers, providing background reference, were all either nominally undoped or lightly doped *p*-type (in the case of boron-doped multilayers on boron-doped substrate).

Dopant profiling was performed on the silicon {110} cross-sections, after the samples were freshly-cleaved in air. Care was taken to ensure that the cleaved specimen exhibited a mirror-like reflective surface with no evident steps in the regions of interest (by visual inspection). Optimised beam parameters achievable on the microscopes were used to analyse doping contrast. As imaging was being performed, the sample stage was positioned such that the beam was incident normally on the cleaved cross-section, and

rastered in a direction perpendicular to the doping junctions (Figure 1). The doped regions of interest were scanned with the electron or helium ion probe only once in order to avoid contamination or charging effects.

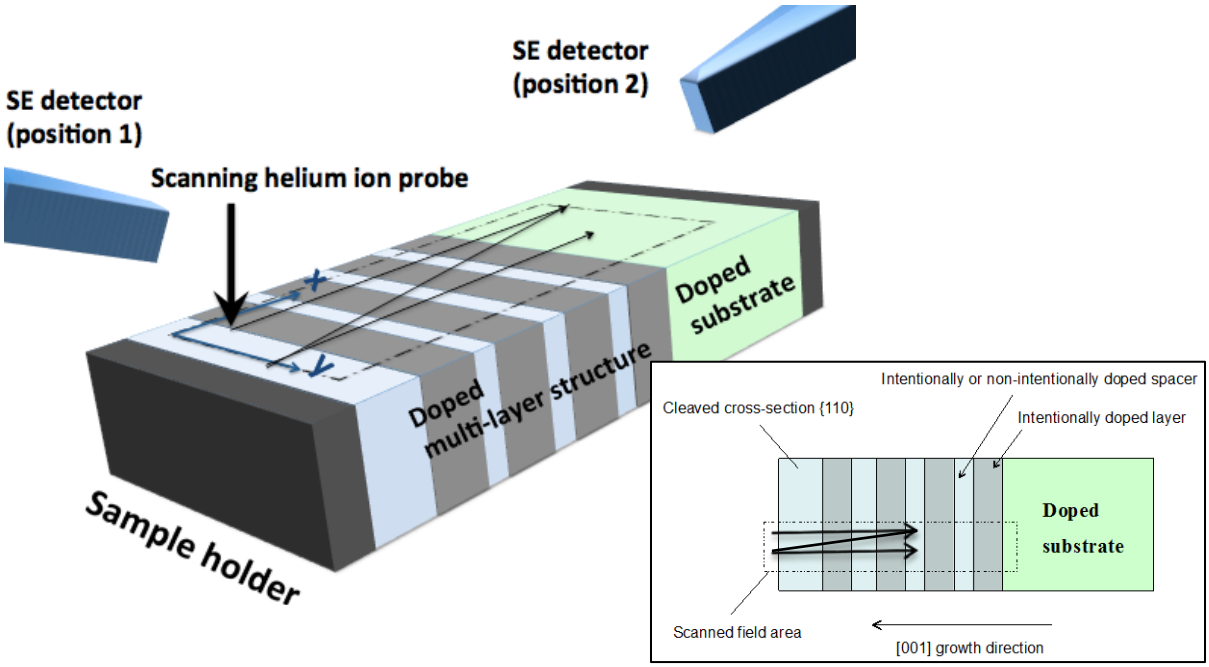

Figure 1: *Schematic of the SHIM imaging procedure of the semiconductor junctions. Two different positions are shown of the SE (Everhart-Thornley or EHT) detector with respect to the sample when the in-plane orientation offsets by 180°. The inset shows the general structure of the doped silicon sample, and sample orientation with respect to the normally incident scanning electron (helium ion) beam in the SEM (SHIM). The arrows indicate the direction of the raster scan, perpendicular to the doping junctions. In the SEM, the through-the-lens detector (TLD) is used for SE detection.*

The SEM was an FEI XL30^{TM} sFEG. The beam accelerating voltage was 1 kV, the probe current was ~ 32 pA and probe diameter was ~ 16 nm. An objective aperture of 30 µm diameter was used, and the pressure in the vacuum chamber using an oil-free turbo-pump system was 3×10^{-6} mbar. Imaging was performed in the ultra-high resolution (UHR) mode using the through-the-lens detector (TLD) system at a working distance of ~ 4 - 6 mm. The extraction and deflection voltages were 20 V and 60 V respectively, which are standard operating conditions for SE imaging. Energy-filtering of the SEs is required to map out donor distributions at high resolution in the SEM. When energy-filtering was applied, the extraction voltage was 250 V and the deflection voltage was specified below 60 V, allowing SEs having energies up to the cut-off energy set by the deflection voltage to pass through and generate the energy-filtered doping contrast image.

The SHIM was a Carl Zeiss Orion® Plus. The beam accelerating voltage was 30 kV, the probe current was ~ 1.2 pA and probe diameter was ~ 0.8 nm. An objective aperture of 10 µm diameter was used, and the pressure in the vacuum chamber using an oil-free turbo-pump system was ~ 5×10^{-7} mbar. Imaging was performed using the Everhart-Thornley (EHT) detector grid biased at 500 V at a working distance of ~ 6 – 8 mm.

In the SEM and SHIM, all the images (712 × 484 pixels) were digitally acquired at a magnification of between 8000 × to 20000 × and a scan frequency of ~ 0.1 frame s^{-1},

and stored as 8-bit datasets. The data were processed using a Java plug-in written for ImageJ™ (Schneider *et al.,* 2012). Line profiles across the regions of interest were row-averaged over at least 100 pixels perpendicular to the scan direction to yield contrast profiles. The doping contrast value C was determined by normalising the SE intensity from the region of interest to that from the doped substrate using our standard formula (Chee *et. al.*, 2011).

$$C = \begin{cases} \dfrac{\Delta I}{\dot{I}_d} = \dfrac{I_d - \bar{I}_{sub}}{I_d - I_0} \quad ; \; if \quad I_d > \bar{I}_{sub} \\ \\ \dfrac{\Delta I}{\dot{I}_{sub}} = \dfrac{I_d - \bar{I}_{sub}}{\bar{I}_{sub} - I_0} \quad ; \; if \quad \bar{I}_{sub} > I_d \end{cases} \tag{1}$$

I_d is the column-averaged SE intensity from the layer of interest, $\bar{I}_{sub}$ is the mean SE intensity from the substrate, and I_0 is the spurious background intensity obtained by blanking out the primary beam. $\Delta I = I_d - \bar{I}_{sub}$ is the absolute intensity difference and $\dot{I}_d$ or $\dot{I}_{sub}$ is the absolute intensity from the respective doped semiconductor layer or substrate regions. The contrast value lies within $-1 \le C \le 1$ using equation 1. The case $C = 0$ represents equivalent SE intensities from the layer/substrate regions, whereas $C = 1$ or $C = -1$ indicates absolute zero yield from the substrate ($\dot{I}_{sub} = 0$) or the layer of interest ($\dot{I}_d = 0$) respectively. Therefore the absolute contrast value is independent of the contrast and brightness settings on the microscope control console.

III. RESULTS AND ANALYSIS

Doping contrast from *p*-type semiconductor

The boron-doped *p*-layer structures shown in Figure 2, have been grown on an antimony-doped *n*-type silicon substrate. The capping and the spacer silicon layers are nominally undoped. The SHIM and SEM experimental profiles have been overlaid for comparison.

Doping contrast, referred to the *n*-substrate, increases monotonically with dopant density, and as shown in Figure 2(a), this contrast is stronger at high acceptor concentrations (~ 3 × 10^{19} dopants cm^{-3}) in the SHIM compared to the SEM; the sensitivity of both techniques to measure doping changes is similar otherwise. Below 10^{18} acceptors cm^{-3}, the *p*-layers (layers D and E) are not discernible from the adjacent undoped spacer layers in the SHIM. Nevertheless, the effect of the placement of the SE detector off-axis to the specimen (Figure 1) may be a factor in this doping contrast as will be evident below.

For the specimen shown in Figure 2 (b), doping contrast is stronger from all the *p*-layers using the SEM technique; in this instance the in-plane sample orientation is offset by 180° in the SHIM (see Figure 1). Under this condition, the SEM provides higher sensitivity to doping variations compared to the SHIM for the range of doping levels

measured. By comparing Figures 2 (a) and (b), it can be seen that the SE doping contrast in the SHIM is not commensurate with acceptor concentration, and we believe this is due to the off-axis detector effect. Although we observed that dopant profiling in the SHIM is largely independent of magnification and grid bias voltage of the EHT detector above 50 V, varying the in-plane sample orientation with respect to the in-chamber EHT detector can substantially modify doping contrast. This procedure demonstrates that without the necessary calibration schemes, quantitative SHIM dopant profiling is not amenable because doping contrast is dependent on the feature geometry and the in-chamber EHT detector orientation with respect to the specimen. As the SEM technique uses a rotationally symmetric TLD for SE detection, asymmetric effects are minimised, and hence doping contrast correlates with the acceptor density within uncertainty limits.

Furthermore, we observed that, for all in-plane sample orientations, the SHIM technique is unable to detect the 100 nm thick *p*-layer having a concentration of 2×10^{17} acceptors cm^{-3} embedded between the intrinsic layer and *n*-substrate (see Figure 2(b)). This may indicate that the resulting free hole distribution in the *p*-type material – following *e.g.* charge compensation due to electrons diffusing from the *n*-substrate – and hence its effect on the electric potentials, is below the detection limit of the SHIM technique. The mechanism responsible for the detection limit will be discussed later. In comparison, the SEM technique has superior sensitivity to low acceptor concentrations, as this same *p*-layer is distinguishable in the image with high resolution. A sensitivity limit as low as about 5×10^{14} dopants cm^{-3} or $\sim 10^{-6}$ atomic % has been demonstrated in a separate study involving *p-n* junction samples in the SEM (see Chee, 2009).

The next figure shows another difference in the properties of SE doping contrast in the SHIM and SEM. Figure 2 (c) compares doping contrast from specimens having *p*-layers of the same doping concentration (10^{19} dopants cm^{-3}) but different dose levels as reflected in the range of layer thicknesses (120 nm, 270 nm and 550 nm). The maximum doping contrast from these *p*-layers is approximately the same either in the SHIM or SEM.

Finite-element simulations were performed to solve Poisson's equation and determine the electric potential energy as a function of depth for the silicon sample used in the experiments above. All edges of the specimen were grounded except for the surface plane exposed to the incident He^+ ion or electron probe. The main surface states on the silicon are silicon-silicon dioxide interface states. To simulate the presence of these surface states, Poisson's equation is modified to account for the trapped charges. A surface state density of 4×10^{12} cm^{-2} was used in the simulations, having amphoteric energy levels localised in the silicon bandgap of 0.38 eV from the band edges, as discussed in (Chee *et al.*, 2011). Figure 2 (c) shows that the SEM cross-sectional experimental profile corresponds most closely to the electric potential distribution at a depth of 5 to 10 nm below the surface, whereas the SHIM technique's profile closely matches the potential energy distribution at a depth of 1 to 3 nm below the surface. At these depths, both the widths and relative heights of the experimental and theoretical curves agree reasonably well; this comparison is ignored in the capping layer due to strong edge-effects resulting in artefacts from the relatively high energy of the He^+ beam (30 keV) and the position-sensitivity due to the off-axis in-chamber EHT detector. The above result is consistent with the fact that, in the SEM, the majority of the SEs escaping from silicon come from within a depth of about 7 nm (Goldstein *et al.*, 2003; Howie, 1995), and in the SHIM, the majority of the SEs escaping come from a depth of about 0.7

– 2.5 nm (Ramachandra *et al.*, 2009). In the former case, these SEs therefore experience a potential distribution within a surface layer about 7 nm deep, and in the latter, the SHIM experimental profile characterises the electric potential in the thin surface layer about 0.7 to 2.5 nm deep, modified by surface band-bending. For reasons that may be due to differences in surface charging and the solid collection angle of the in-chamber EHT detector, the position of the electrical junction determined by the SHIM technique is different from that of the SEM.

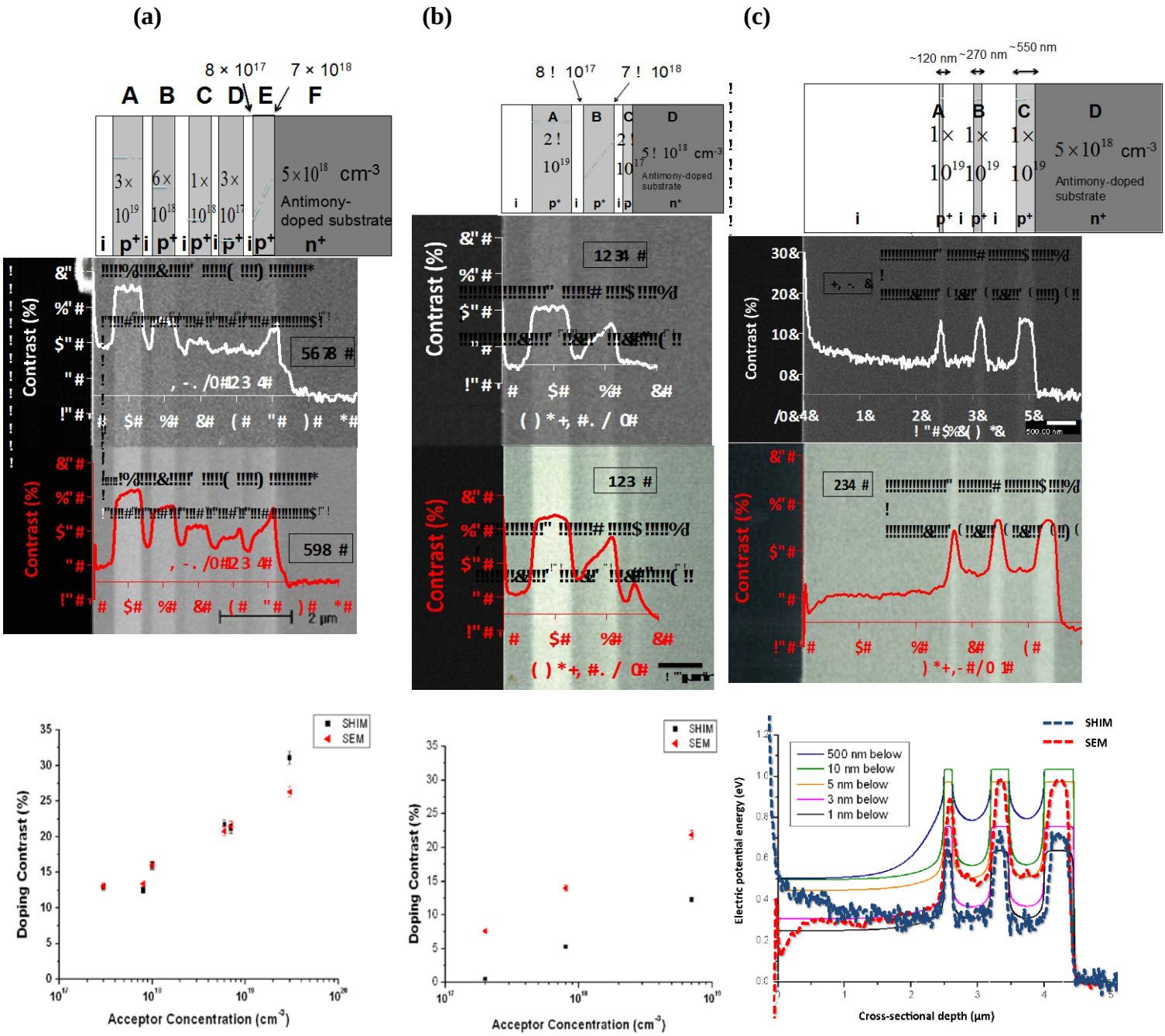

Figure 2: *SHIM and SEM doping contrast from the silicon specimen: (a) comprising five boron-doped layers (layer width ~ 800 nm) with acceptor concentrations ranging from 8 × 10^{18} to 2 × 10^{16} dopants cm^{-3}; (b) comprising three boron-doped layers with layer widths ranging from 100 nm to 1 um and acceptor concentrations ranging from 2 × 10^{17} to 2 × 10^{19} dopants cm^{-3}; and (c) comprising three boron-doped layers each with an acceptor concentration of 10^{19} dopants cm^{-3} and layer widths ranging from 120 to 560 nm. The experimental uncertainty is ± 3 % of the data points. Also included is the energy distribution (electric potential with respect to the substrate) across the specimen at various depths below the cross-sectional surface, i.e. 1 nm, 3 nm, 5 nm, 10 nm and 500 nm, the latter being essentially in bulk material, grown on an n-type silicon substrate antimony-doped to 5 × 10^{18} dopants cm^{-3}. The SHIM and SEM experimental curves are superimposed for comparison.*

Figure 3 shows a boron-doped *p*-layer structure grown on a lightly boron-doped *p*-substrate. The capping and spacer layers have boron doping to a concentration of 10^{17} acceptors cm^{-3}. Such a specimen may test the technique's sensitivity to measure acceptor concentration variations without a *p*-*n* junction. Predictably, because of the smaller potential difference, the doping contrast from the *p*-layer (with respect to the *p*-substrate) is reduced compared to specimens having a *p*-*n* junction (*i.e.* measured with respect to the *n*-substrate).

Owing to its sensitivity being limited to above 10^{17} acceptors cm^{-3}, and with the detector position a factor, the SHIM technique is unable to measure the doping in layer C or its adjacent spacer layers despite an acceptor density approaching three orders of magnitude higher than that in the *p*-substrate (see Figure 3). On the contrary, the sensitivity of the SEM technique to measure acceptor concentration variations is generally superior to that of the SHIM for the doping levels studied. The spacer layers can be distinguished from the *p*-substrate, indicating that a step change of approximately 10^{17} acceptors cm^{-3} or more can be measured against a *p*-substrate concentration of 5×10^{14} acceptors cm^{-3}. Nevertheless, the SEM is unable to reliably measure a step change in doping of 5×10^{16} acceptors cm^{-3} or less, such as between layer C and the adjacent spacer layers under the specific conditions of this study.

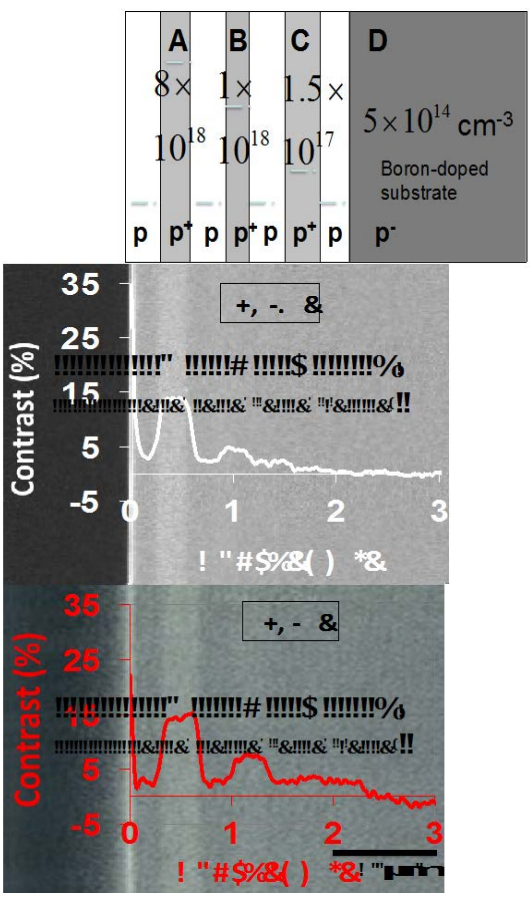

Figure 3: *SHIM and SEM doping contrast from the silicon specimen comprising three boron-doped p-type silicon layers (layer width ~ 400 nm) having acceptor concentrations ranging from 1.5 × 10^{17} to 8 × 10^{18} dopants cm^{-3}, epitaxially grown on a p-type silicon substrate boron-doped to 5 × 10^{14} dopants cm^{-3}. The capping and spacer silicon layers are boron-doped to 10^{17} dopants cm^{-3}.*

Doping contrast from *n*-type semiconductor

Figure 4 (a)-(c) shows an *n*-layer silicon structure, where the phosphorus-doped layers have been grown on a boron-doped *p*-type silicon substrate; this type of specimen involves a *p*-*n* junction. The contrast from the *n*-layers is significantly higher in the SHIM compared to the SEM, but the resolution is limited by layer C, as it is barely distinguishable from the adjacent undoped layer (see Figure 4(b)). Hence, again taking position-sensitive detection in the SHIM into account, we observe that the minimum measureable change in donor concentration is just under 10^{18} donors cm^{-3} with respect to the undoped semiconductor, but as low as 3×10^{16} donors cm^{-3} at the *p*-*n* junction.

Nevertheless, all the *n*-layers, including layer C, are distinguishable from the adjacent spacer layers in the SEM dopant map (see Figure 4 (c)). Figure 4 (d) summarises the contrast values from the *n*-layers, normalised to the *p*-substrate, as a function of the donor density. This doping contrast is negatively related to the number of donors, and it is clear that the SHIM technique is more sensitive to changes in donor concentrations compared to that of the SEM.

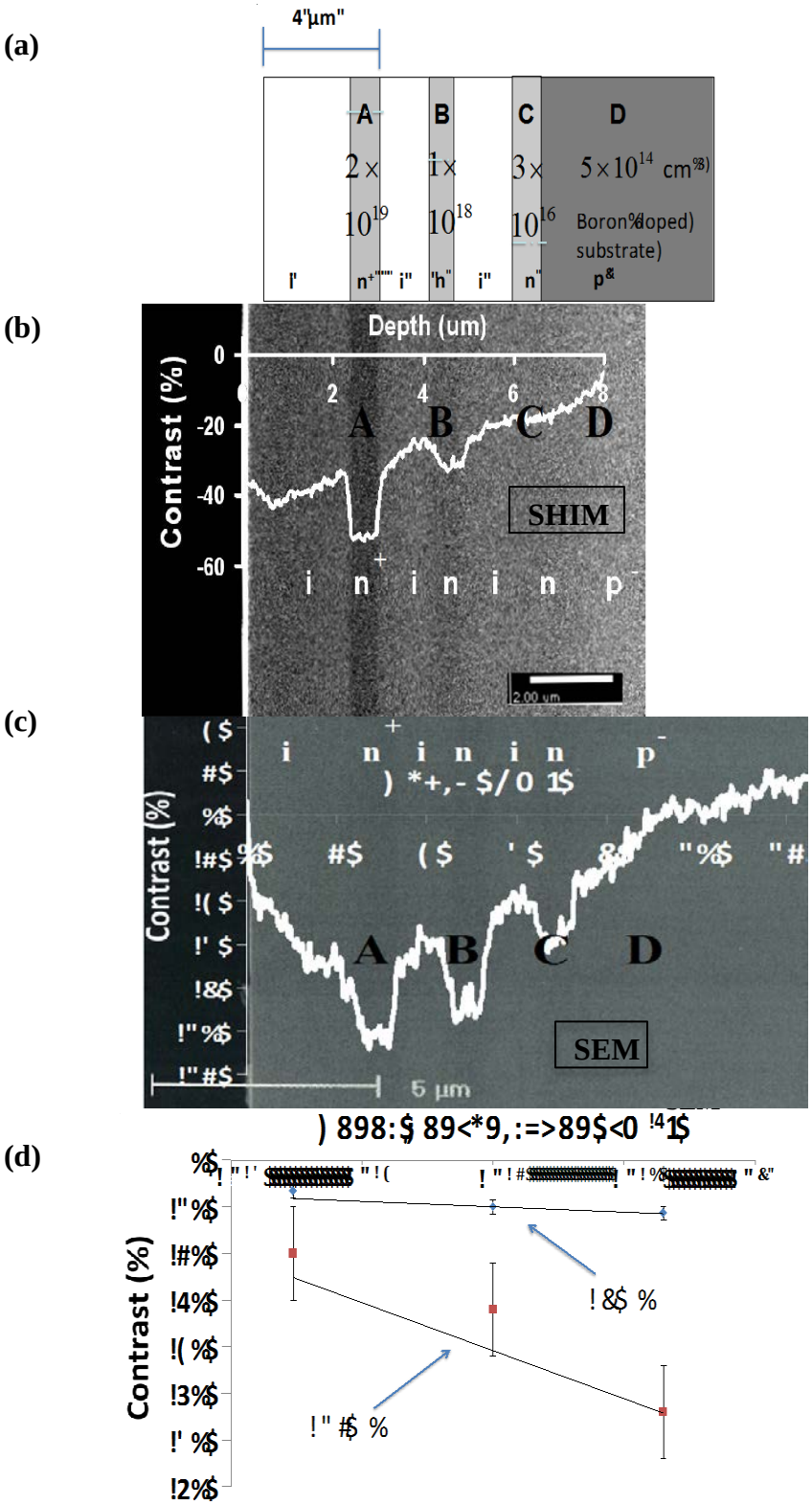

Figure 4: *(a) Doping structure comprising phosphorus-doped silicon layers (layer width ~ 800 nm). The donor concentrations measured by SIMS for the n-layers labelled A, B and C were ~2.0 × 10^{19} cm^{-3}, ~ 10^{18} cm^{-3} and ~3.0 × 10^{16} cm^{-3} respectively. Region D is the boron-doped p-type silicon substrate having ~5.0 × 10^{14} acceptors cm^{-3}. Doping contrast in an b) SHIM or c) SEM. d) Doping contrast values of the n-layers normalised to the p-substrate in the SHIM or SEM. The experimental uncertainty is ±10 % and ±1.5 % for the SHIM and SEM respectively.*

Figure 5(a) shows an *n*-layer silicon structure, where the phosphorus-doped layers have been grown on an antimony-doped *n*-type silicon substrate. This structure may test the technique's ability to detect and measure donor concentration variations on specimens without a *p*-*n* junction.

In the SHIM, energy-filtering is not needed for strong doping contrast to be observed from *n*-layers having above 10^{17} donors cm^{-3} (Figure 5 (b)). Nevertheless, the contrast is not commensurate with donor concentration: whilst there is strong doping contrast from the *n*-*i* junctions, the contrast values do not correspond to the relative donor concentrations. Since the SEs emitted from *n*-type regions have the lowest kinetic energies, the SHIM technique is especially sensitive to the feature geometry and the specimen orientation with respect to the off-axis detector. Therefore, although donor localisation is possible, quantification of donor profiles for this type of specimens is not yet viable in the SHIM.

When operating the SEM under standard imaging conditions, doping contrast cannot be used to adequately distinguish the *n*-layers as that shown in Figure 5 (c) (see also Schonjahn *et al.*, 2002; Chee, 2009). To dramatically improve sensitivity to donor concentrations and to allow their mapping and quantification at high resolution (Figure 5 (d)), low-pass energy-filtering of the SEs is essential, in which case high extraction fields (> 1 $kVcm^{-1}$) are required from the TLD.

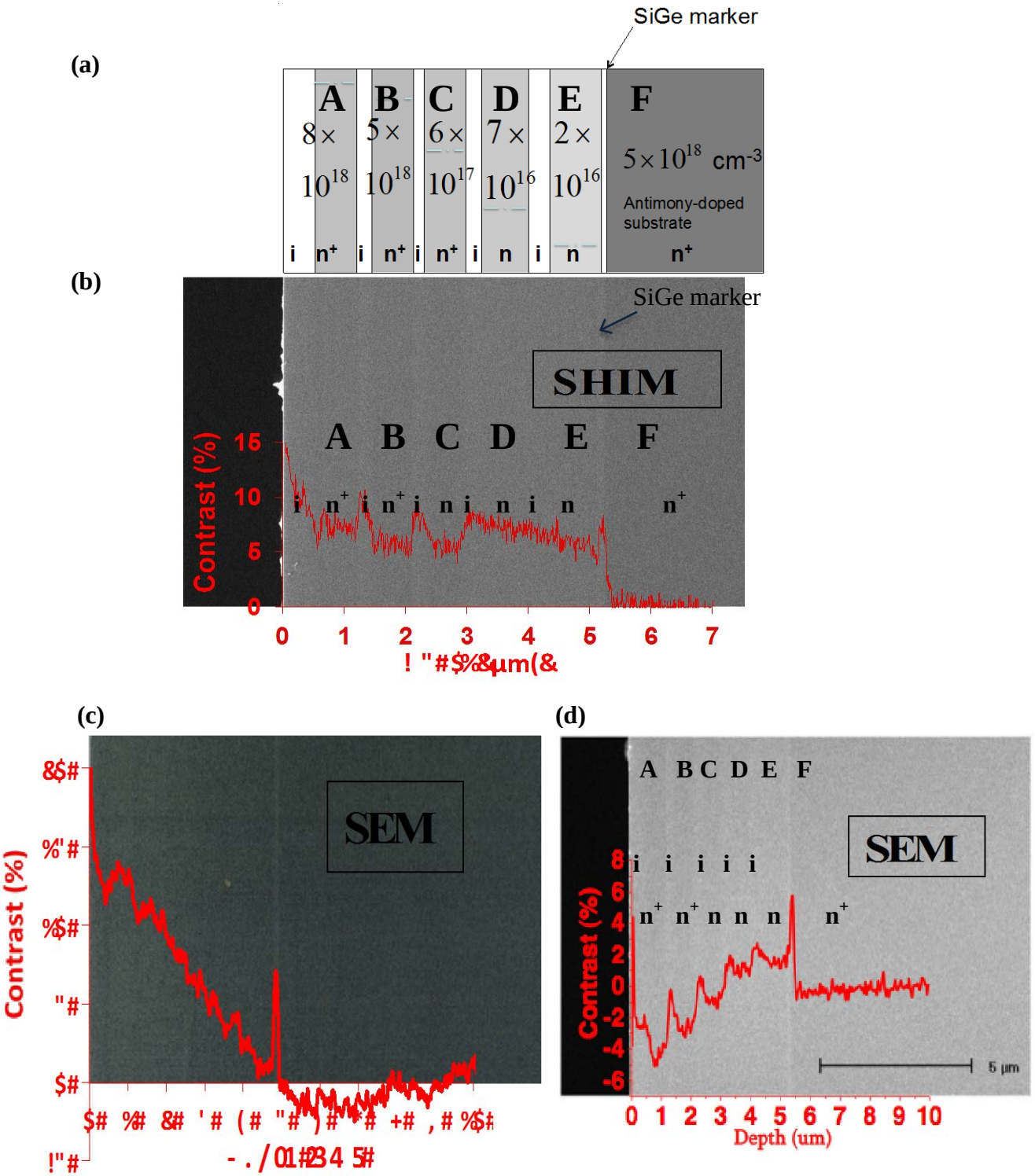

Figure 5: *(a) Doping structure comprising phosphorus-doped layers (layer width ~ 800 nm) with concentrations ranging from 2 × 10^{16} to 8 × 10^{18} donors cm^{-3}, and a silicon-germanium marker layer, epitaxially grown on an n-type silicon substrate antimony-doped to 5 × 10^{18} dopants cm^{-3}. Doping contrast in an (b) SHIM under standard imaging conditions; and in an SEM (c) under standard imaging conditions without energy-filtering and (d) with energy-filtering at a deflection voltage of 20 V.*

IV. DISCUSSION AND CONCLUSIONS

The SE doping contrast technique based on the SHIM or SEM has been studied on a range of *p*- and *n*-layer silicon structures having step changes in dopant concentrations. The sensitivity and quantification accuracy of each technique depends on, whether acceptors or donors are to be mapped, the substrate doping, and in some cases, the feature geometry and sample orientation.

In the SHIM, stronger doping contrast can be achieved than in the SEM for high acceptor concentrations 3×10^{19} cm^{-3} or above on samples that have an *n*-type substrate. Below this value, the sensitivity to changes in the number of acceptors is approximately the same for both techniques, but limited by the SHIM's threshold sensitivity to low acceptor concentrations. Additionally, our study has shown that the sensitivity to acceptor density changes may be reduced in the SHIM depending on the sample orientation with respect to the in-chamber EHT detector position. This is an off-axis detector effect, which therefore represents a non-trivial problem for quantification.

As shown in studies of the *p*-layers on the *p*-substrate, the SEM is able to map out acceptor concentrations as low as ~ 5×10^{14} cm^{-3}, but it is unable to measure changes of 5×10^{16} cm^{-3} or less. On the other hand, the SHIM is only able to measure changes by at least an order of magnitude higher, above its sensitivity limit of > 2×10^{17} cm^{-3}. For *n*-layer samples on the *p*-substrate, there is a negative correlation of the doping contrast and the donor concentration, wherein no energy-filtering is required. The (SHIM) SEM is (un)able to measure donor concentration changes by as low as 3×10^{16} cm^{-3} from the *n*-*i* junction contrast; yet both techniques are able to measure a donor concentration of this magnitude from the *p*-*n* junction contrast. Donor distributions in specimens without a *p*-*n* junction require specialised low pass energy-filtering techniques to be mapped out at high resolution in the SEM. However, strong doping contrast, highly sensitive to donor concentration changes, can be obtained in the SHIM even without the need for energy-filtering.

The sensitivity limits of the two techniques to low dopant concentrations with and without a *p*-*n* junction are summarised in Table 2.

Acceptor dopant profiling	With *p*-*n* junction	Without *p*-*n* junction
SHIM	> 2×10^{17} cm^{-3}	> 2×10^{17} cm^{-3}
SEM	~ 5×10^{14} cm^{-3} (Chee *et al.*, 2009)	~ 5×10^{14} cm^{-3}

Donor dopant profiling	With *p*-*n* junction	Without *p*-*n* junction
SHIM	< 3×10^{16} cm^{-3}	< 6×10^{17} cm^{-3}
SEM	< 3×10^{16} cm^{-3}	< 2×10^{16} cm^{-3} (energy-filtering employed)

Table 2: Low dopant concentration sensitivity limits of the SEM or SHIM dopant profiling technique on specimens having a *p*-*n* junction or without.

The reason for the poorer sensitivity of the SHIM technique to low dopant concentrations in unfavourable specimens may be surface charging, contamination or damage effects on silicon resulting from the relatively high He^+ beam energy of 30 keV. The resulting surface effects may explain why the doping contrast is observed to be largely

independent of magnification, and why the position of the electrical *p*-*n* junction is displaced significantly compared to the SEM technique in some instances (*e.g.* Figure 2c).

The so-called off-axis detector effect has a large impact on quantitative donor mapping in specimens lacking a *p*-*n* junction. The SHIM technique is particularly sensitive because the emitted SEs have relatively low energy and therefore are highly susceptible to external fields from the detector and/or sample orientation. Another origin of quantification errors may be due to the non-uniform extraction fields extended to the specimen surface from the in-chamber EHT detector. Without a *p*-*n* junction, patch field and angular emission doping contrast mechanisms are weak compared to the influence of these spatially varying extraction fields (see Chee, 2009, Chee *et al.*, 2011). Where the slowest SE emissions from donor distributions are concerned, the above situation leads to feature geometry-dependent results that are artefacts in the dopant map. The SE yields from *p*-type regions have higher energies; hence any quantification errors due to the extraneous detector effects are less significant.

Furthermore, we have shown that the relative widths and heights of the experimental profile from the *p*-layers of silicon using SE imaging in the SEM (SHIM) correspond closely with the relative widths and heights of the energy distribution across these layers, at a depth of 5 to 10 nm (1 to 3 nm) below the surface. This suggests that doping contrast in the SEM (SHIM) is a function of bulk built-in voltages modified by band-bending effects within 5 to 10 nm (1 to 3 nm) of the surface, consistent with the mean escape depth of SEs in silicon being about 7 nm (1.8 nm). Energy-filtering in the SEM is able to produce strong contrast from donor distributions because according to Fitting *et al.* (1984), (2001), the lower kinetic energies of SE emission correspond mostly to SEs that escape from deeper below the surface when induced by a primary electron beam. This has an important consequence because the mean escape depth from *n*-type regions is small relative to that from *p*-type regions due to surface band-bending as a major factor (Fitting and Boyde, 1983). Therefore selecting only the slowest SEs allows the SE yield to be differentiated by doping dependent surface band-bending, which is a mechanism for doping contrast. The SHIM technique does not require energy-filtering to produce strong contrast from donor distributions, because the average kinetic energy of SE emission is much lower compared to the case for the SEM (Petrov and Vyvenko, 2011). In the SHIM technique, most SEs stem from within a thin surface region 0.7 to 2.5 nm deep, and therefore we conclude that is the reason why it is so highly sensitive to donor distributions without the need for energy-filtering.

This study leads to a deeper understanding of the physical mechanisms underpinning SE doping contrast. The application of the SHIM technique is promising in nanoelectronics, where the localisation of a few active dopants in nanometre volumes, which impacts on the electrical performance of heterostructure/homojunction devices, can be mapped out and analysed at high resolution without energy-filtering. Although our studies have shown that accurate quantification of dopant distributions is particularly challenging using the present SHIM technology, our results suggest that improvements in detector instrumentation (*e.g.* in-lens detector design configuration), performing surface charge neutralisation using the electron flood gun, and having lower beam energy functionalities to reduce damage or deposition effects, may enable improved dopant profiling quantification accuracy.

ACKNOWLEDGEMENTS

A.K.W. Chee thanks Professor Sir Colin Humphreys (University of Cambridge) for support and advice during his academic study leave to Southampton, and Professor Harvey Rutt (University of Southampton) is gratefully acknowledged for hosting access to facilities at the Southampton Nanofabrication Centre to carry out this work. The following grants are acknowledged, from NSFC (No. 61650110517) and Ningbo Natural Science Foundation (No. 2014A610154).

References

C. W. Oatley and T. E. Everhart, J. Electron., **2**, 568-570 (1957).

C.P Sealy, M.R. Castell and P. R. Wilshaw, J. Elec. Microsc., **49**(2), 311 – 321 (2000).

A.K.W. Chee, E.G.T Bosch, R. F. Broom and C.J. Humphreys, J. Appl. Phys., **109**, 013109 (2011).

A.K.W. Chee, Ph.D. thesis, University of Cambridge, U.K. (2009).

D.D. Perovic, M.R. Castell, A. Howie, C. Lavoie, T. Tiedje and J.S.W. Cole, Ultramicrosc., **58**, 104-113 (1995).

D. D. Perovic, R. Turan and Castell, M. R., Inst. of Mat.: Int. Cent. Symp. Elect., 258 (1998).

D. Venables, H. Jain and D. C. Collins, J. Vac. Sci. & Tech. B: Microelec. Nano. Struct., **16**, 362 (1998).

S. L. Elliott, R. F. Broom and C. J. Humphreys, J. Appl. Phys., **91**, 9116 (2002).

R. Turan, D. D. Perovic and D. C. Houghton, Appl. Phys. Lett., **69**, 1593 (1996).

M. R. Castell, T. W. Simpson, I. V. Mitchell, D. D. Perovic and J. M. Baribeau, Appl. Phys. Lett., **74**(16), 2304-2306 (1999).

A. K. W. Chee, C. Rodenburg and C. J. Humphreys, Elect. Microsc. Anal., **126**, 012033 (2007).

C.A. Schneider, W.S. Rasband, K.W. Eliceiri, Nature Methods **9**, 671 (2012).

J. A. Notte, United States patent, Appl. No. 11/853471, US 2008/0111069 A1, (15 May 2008).

K. Inai, K. Ohya and T. Ishitani, J. Electron Microsc. **56**, 163 (2007).

B. W. Ward, J. A. Notte and N. P. Economou, J. Vac. Sci. Technol. B **24**, 2871 (2006).

C. Schonjahn, C. J. Humphreys and M. Glick, J. Appl. Phys., **92**,12 (2002).

J. Goldstein, D. Newbury, D. Joy, C. Lyman, P. Echlin, E. Lifshin, L. Sawyer and J. Michael, Scanning Electron Microscopy and X-ray Microanalysis, 3rd ed. (Kluwer Academic/Plenum Publishers, New York) (2003).

A. Howie, Microsc. Microanal. **6**, p 291 (2000).

R. Ramachandra, B. Griffin and D. Joy, Ultramicrosc. **109**, 748–757 (2009).

M.A.E. Jepson, X. Liu, D. Bell, D. Ferranti, B. Inkson and C. Rodenburg, Microsc. Microanal. **17**, 637 (2011).

H. J. Fitting and J. Boyde, Phys. Stat. Sol. (a), **75**(1), (1983).

H. J. Fitting, J. Boyde and J. Reinhardt, Phys. Stat. Sol. (a), **81**(1), (1984).

H. J. Fitting, E. Schreiber, J. C. Kuhr and A. von Czarnowski, J. Elec. Spectrosc. Rel. Phenom., **119**(1), 35-47 (2001).

Y.V. Petrov and O.F. Vyvenko, in Proc. SPIE, Vol. 8036, edited by J.T. Thomas, D.D. Desjardins, J.J. Güell and K. L. Bernier (SPIE, Orlando, Florida, 2011) pp. 80360O–1–80360O–10 (2011).